



Summary of Publications: Single-Edge Tension SE(T) Tests

Report 277-T-04

for Project

Weld Design, Testing, and Assessment Procedures for High Strength Pipelines

Prepared for the

Design, Materials, and Construction Technical Committee of
Pipeline Research Council International, Inc.
Project MATH-1 Catalog No. L5XXXX

and

U.S. Department of Transportation
Pipeline and Hazardous Materials Safety Administration
Office of Pipeline Safety
Agreement Number DTPH56-07-T-000005

Prepared by

W.R. Tyson, G. Shen, J.A. Gianetto and D.Y. Park
CANMET Materials Technology Laboratory

September 2011

This research was funded in part under the Department of Transportation, Pipeline and Hazardous Materials Safety Administration's Pipeline Safety Research and Development Program. The views and conclusions contained in this document are those of the authors and should not be interpreted as representing the official policies, either expressed or implied, of the Pipeline and Hazardous Materials Safety Administration, or the U.S. Government.

CANMET Materials Technology Laboratory

Summary of Publications: Single-Edge Tension SE(T) Tests

W.R Tyson, D.Y. Park, J.A. Gianetto and G. Shen

CANMET Materials Technology Laboratory
Minerals and Metals Sector, Natural Resources Canada
183 Longwood Road South, Hamilton, ON, Canada, L8P 0A5

CANMET REPORT No. 2010-26(TR)

September 2011

DISCLAIMER

Natural Resources Canada makes no representations or warranties respecting the contents of this report, either expressed or implied, arising by law or otherwise, including but not limited to implied warranties or conditions of merchantability or fitness for a particular purpose.



Catalog No. L5XXXX

Summary of Publications: Single-Edge Tension SE(T) Tests

Report 277-T-04

for Project

Weld Design, Testing, and Assessment Procedures for High Strength Pipelines

Prepared for the

Design, Materials, and Construction Technical Committee of
Pipeline Research Council International, Inc.
Project MATH-1 Catalog No. L5XXXX

and

U.S. Department of Transportation
Pipeline and Hazardous Materials Safety Administration
Office of Pipeline Safety
Agreement Number DTPH56-07-T-000005

Prepared by

W.R. Tyson, G. Shen, J.A. Gianetto and D.Y. Park
CANMET Materials Technology Laboratory

Version	Date of Last Revision	Date of Uploading	Comments
Draft	November 2010	8 April 2011	
Final	January 2012		

This report is furnished to Pipeline Research Council International, Inc. (PRCI) under the terms of PRCI contract [277-PR-348-074512], between PRCI and the MATH-1 contractors:

- Electricore (prime contractor),
- Center for Reliable Energy Systems, CANMET, NIST, and The Lincoln Electric Company (sub-contractors).

The contents of this report are published as received from the MATH-1 contractor and subcontractors. The opinions, findings, and conclusions expressed in the report are those of the authors and not necessarily those of PRCI, its member companies, or their representatives. Publication and dissemination of this report by PRCI should not be considered an endorsement by PRCI of the MATH-1 contractor and subcontractors, or the accuracy or validity of any opinions, findings, or conclusions expressed herein.

In publishing this report, PRCI and the MATH-1 contractors make no warranty or representation, expressed or implied, with respect to the accuracy, completeness, usefulness, or fitness for purpose of the information contained herein, or that the use of any information, method, process, or apparatus disclosed in this report may not infringe on privately owned rights. PRCI and the MATH-1 contractors assume no liability with respect to the use of, or for damages resulting from the use of, any information, method, process, or apparatus disclosed in this report. By accepting the report and utilizing it, you agree to waive any and all claims you may have, resulting from your voluntary use of the report, against PRCI and the MATH-1 contractors.

Pipeline Research Council International Catalog No. L5XXXX

PRCI Reports are Published by Technical Toolboxes, Inc.

3801 Kirby Drive, Suite 520
Houston, Texas 77098
Tel: 713-630-0505
Fax: 713-630-0560
Email: info@ttoolboxes.com

PROJECT PARTICIPANTS

PROJECT TEAM MEMBER	COMPANY AFFILIATION	PROJECT TEAM MEMBER	COMPANY AFFILIATION
Arti Bhatia	Alliance	Jim Costain	GE
Jennifer Klementis	Alliance	Gilmar Batista	Petrobras
Roger Haycraft	Boardwalk	Marcy Saturno de Menezes	Petrobras
David Horsley	BP	Dave Aguiar	PG&E
Mark Hudson	BP	Ken Lorang	PRCI
Ron Shockley	Chevron	Maslat Al-Waranbi	Saudi Aramco
Sam Mishael	Chevron	Paul Lee	SoCalGas
David Wilson	ConocoPhillips	Alan Lambeth	Spectra
Satish Kulkarni	El Paso	Robert Turner	Stupp
Art Meyer	Enbridge	Gilles Richard	TAMSA
Bill Forbes	Enbridge	Noe Mota Solis	TAMSA
Scott Ironside	Enbridge	Philippe Darcis	TAMSA
Sean Keane	Enbridge	Dave Taylor	TransCanada
Laurie Collins	Evraz	Joe Zhou	TransCanada
David de Miranda	Gassco	Jason Skow	TransGas
Adriaan den Herder	Gasunie	Ernesto Cisneros	Tuberia Laguna
Jeff Stetson	GE	Vivek Kashyap	Welspun
		Chris Brown	Williams

CORE RESEARCH TEAM	
RESEARCHER	COMPANY AFFILIATION
Yaoshan Chen	Center for Reliable Energy Systems
Yong-Yi Wang	Center for Reliable Energy Systems
Ming Liu	Center for Reliable Energy Systems
Dave Fink	Lincoln Electric Company
Marie Quintana	Lincoln Electric Company
Vaidyanath Rajan	Lincoln Electric Company
Joe Daniel	Lincoln Electric Company
Radhika Panday	Lincoln Electric Company
James Gianetto	CANMET Materials Technology Laboratory
John Bowker	CANMET Materials Technology Laboratory
Bill Tyson	CANMET Materials Technology Laboratory
Guowu Shen	CANMET Materials Technology Laboratory
Dong Park	CANMET Materials Technology Laboratory
Timothy Weeks	National Institute of Standards and Technology
Mark Richards	National Institute of Standards and Technology
Dave McColskey	National Institute of Standards and Technology
Enrico Lucon	National Institute of Standards and Technology
John Hammond	Consultant Metallurgist & Welding Engineer

This Page Intentionally Left Blank

FINAL REPORT STRUCTURE

Focus Area 1 - Update of Weld Design, Testing, and Assessment Procedures for High Strength Pipelines		
Report #	Description	Lead Authors
277-T-01	Background of Linepipe Specifications	CRES/CANMET
277-T-02	Background of All-Weld Metal Tensile Test Protocol	CANMET/Lincoln
277-T-03	Development of Procedure for Low-Constraint Toughness Testing Using a Single-Specimen Technique	CANMET/CRES
277-T-04	Summary of Publications: Single-Edge Notched Tension SE(T) Tests	CANMET
277-T-05	Small Scale Tensile, Charpy V-Notch, and Fracture Toughness Tests	CANMET/NIST
277-T-06	Small Scale Low Constraint Fracture Toughness Test Results	CANMET/NIST
277-T-07	Small Scale Low Constraint Fracture Toughness Test Discussion and Analysis	CANMET/NIST
277-T-08	Summary of Mechanical Properties	CANMET
277-T-09	Curved Wide Plate Tests	NIST/CRES
277-T-10	Weld Strength Mismatch Requirements	CRES/CANMET
277-T-11	Curved Wide Plate Test Results and Transferability of Test Specimens	CRES/CANMET
277-S-01	Summary Report 277 Weld Design, Testing, and Assessment Procedures for High Strength Pipelines	CRES

Focus Area 2 - Development of Optimized Welding Solutions for X100 Linepipe Steel		
Report #	Description	Lead Authors
278-T-01	State of The Art Review	Lincoln
278-T-02	Material Selection, Welding and Weld Monitoring	Lincoln/CANMET
278-T-03	Microstructure and Hardness Characterization of Girth Welds	CANMET/Lincoln
278-T-04	Microstructure and Properties of Simulated Weld Metals	CANMET/Lincoln
278-T-05	Microstructure and Properties of Simulated Heat Affected Zones	CANMET/Lincoln
278-T-06	Essential Welding Variables	Lincoln/CANMET
278-T-07	Thermal Model for Welding Simulations	CRES/CANMET
278-T-08	Microstructure Model for Welding Simulations	CRES/CANMET
278-T-09	Application to Other Processes	Lincoln/CANMET
278-S-01	Summary Report 278 Development of Optimized Welding Solutions for X100 Line Pipe Steel	Lincoln

EXECUTIVE SUMMARY

This is the third report of a series of seven technical reports detailing the small-scale mechanical testing performed on the trial welds in this consolidated program. An outline of the reporting flow is given in the Introduction to the Summary of Mechanical Properties technical report 277-T-08. The present report highlights the principal results of preliminary application of the toughness test procedure that have been published in a series of papers in the open literature.

A low-constraint test designed to reduce unnecessary conservatism in the measurement of toughness for use in the assessment of flaws in pipeline girth welds has been developed at CANMET Materials Technology Laboratory (CANMET–MTL). The test was first proven on nominally homogeneous material (pipe base metal) to check the practicality of the procedures and to study the effects of the controlling geometric parameters (a/W , etc.) on toughness. The intent of this report is to reference the publications resulting from this work and to summarize the principal conclusions.

TABLE OF CONTENTS

EXECUTIVE SUMMARY	viii
TABLE OF CONTENTS.....	ix
LIST OF FIGURES	x
LIST OF TABLES	x
1 CRACK DRIVING FORCE [1].....	1
2 EFFECT OF BIAXIAL STRESS ON RESISTANCE CURVE [2].....	2
3 FRACTURE TOUGHNESS OF HIGH STRENGTH STEEL PIPE: CONSTRAINT MATCHING [3].....	4
4 CRACK SIZE MEASUREMENT USING UNLOADING COMPLIANCE [4]	6
5 TRIALS USING SE(T) PROCEDURE [5].....	10
6 EVALUATION OF CTOD FROM J-INTEGRAL FOR SE(T) SPECIMENS [6].....	11
7 EFFECT OF SIDE GROOVES [7].....	13
8 CRACK GROWTH CORRECTION [8]	14
9 FRACTURE TOUGHNESS OF X100 PIPE STEEL: SE(B) AND SE(T) SPECIMENS, ROOM TEMPERATURE AND -20°C [9]	15
10 STRETCH ZONE AND BLUNTING LINE [10].....	17
11 SUMMARY	18
12 REFERENCES	19

LIST OF FIGURES

Figure 1. Thin-walled pipe with a circumferential crack under axial tension and internal pressure	1
Figure 2. J-integral for pipe with a circumferential crack as a function of axial strain	2
Figure 3. J-resistance curves for 2D SE(B) and SE(T) samples, $a/t=0.5$	3
Figure 4. J-resistance curves evaluated for pipe with circumferential crack subjected to axial tension and internal pressure (3D model).	3
Figure 5. Crack-tip opening stress for an external axisymmetric crack in a pipe (2-D), $a/t=0.5$, $H/D=10$	4
Figure 6. Crack-tip opening stress for SE(T) clamped sample, $a/W=0.5$, $H/D=10$	5
Figure 7. Crack-tip opening stress for SE(B) samples, $a/W=0.5$	5
Figure 8. J - Q relations for pipe and SE(T) samples	6
Figure 9. SE(T) specimen under load	7
Figure 10. CMOD compliance versus applied load evaluated by FEA	8
Figure 11. J-R curves for an X-100 pipe steel, no rotation correction, PS: plain-sided; SG: side-grooved	9
Figure 12. J-R curves for an X-100 pipe steel, with rotation correction and a_{oq} adjustment, PS: plain-sided; SG: side-grooved	9
Figure 13. Crack size for clamped SE(T) specimens. a_o , a_f : initial and final crack size (SG: side-grooved, PS: plain-sided)	10
Figure 14. J-R curves measured using SE(T) and SE(B) specimens, $a/W=0.5$	11
Figure 15. Factor m as function of applied load for a deep crack	12
Figure 16. Values of m for SE(T) at load $P \leq P_Y$ and for SE(B) at $\delta_{max}=a/20$	13
Figure 17. Distribution of J-integral along the crack front , $a/W=0.2$, 10% side grooves	14
Figure 18. J-resistance curve for X100 pipe steel, with correction for crack growth according to improved procedure (Tyson) and conventional procedure (ASTM) at crack size intervals of 0.016b, 0.032b, and 0.064b	15
Figure 19. J-resistance curves for SE(T) specimens tested at -20°C , side grooved (SG) 10% (5% on each side)	16
Figure 20. Examples of uneven crack growth in tension specimens: LHS - total 10% side-grooved, shallow-cracked ($a/W \cong 0.25$) specimen and RHS - total 20% side-grooved, deeply-cracked ($a/W \cong 0.5$) specimen. The root radius of side grooves on both specimens is 0.5 mm.	16
Figure 21. J at $\Delta a=0.5$ mm versus initial crack length ($a/W=0.25$ and 0.5) for plain-sided (PS) tension and bend specimens at room temperature	17

LIST OF TABLES

Table 1. J values (kJ/m^2) at $\Delta a=0.5$ mm	11
Table 2. Values of $2\tan\theta$ (=k)	18

1 CRACK DRIVING FORCE [1]

The crack driving force is normally taken to be either the J-integral or the crack-tip opening displacement (CTOD or δ). It was decided in this work to focus primarily on the J-integral because of its robustness and greater ease of calculation. However, since the preference in the pipeline industry is for the use of CTOD, this parameter was also calculated periodically.

To become familiar with the principal issues, a finite element analysis (FEA) of the driving force on a circumferential flaw in a pipe under simultaneous axial tensile stress and internal pressure was conducted. A stress-strain equation of Ramberg-Osgood type with $N=10$ was used. The geometry is shown in Figure 1; parameters chosen were $a/t=0.5$, $t/R_i=20$, $pR_i/\sigma_0t=0.25$, 0.50 and 0.75 where the symbols have their usual meaning.

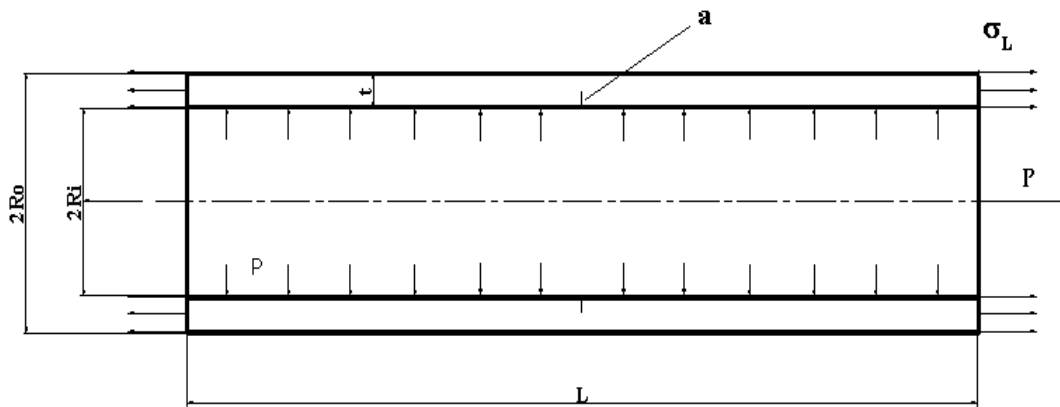


Figure 1. Thin-walled pipe with a circumferential crack under axial tension and internal pressure

The results showed that the J-integral increases with internal pressure at a given axial strain as shown in Figure 2. The reason for this is that as the secondary (hoop) stress σ_T increases while the axial strain is held constant, the axial stress must increase according to the yield criterion.

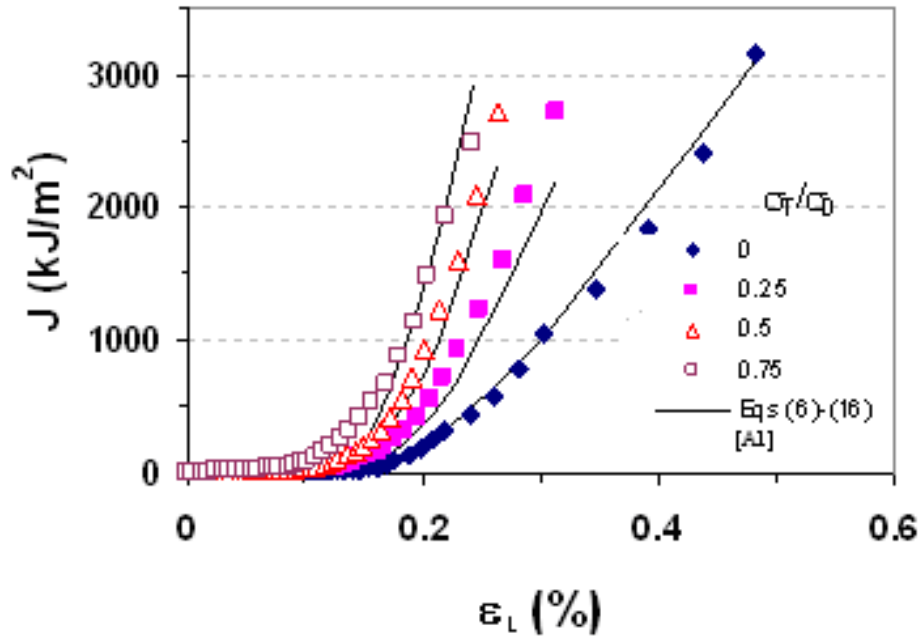


Figure 2. J-integral for pipe with a circumferential crack as a function of axial strain

It was concluded that the effect of a secondary stress should not be neglected in strain-based design.

2 EFFECT OF BIAXIAL STRESS ON RESISTANCE CURVE [2]

As noted above, there is a significant effect of a biaxial stress on the crack driving force for a circumferential flaw in a pipe under tension. It is then logical to ask whether a biaxial stress has a similar effect on the material resistance, or R curve.

The effect of such a secondary stress parallel to the crack front on resistance to ductile tearing was studied by finite element simulation using the Gurson-Tvergaard-Needleman (GTN) model. Values of GTN parameters typical of modern line pipe steels were chosen. Crack initiation and propagation for a 3D standard single edge bending (SE(B)) sample under three-point bending with and without biaxial (out-of-plane) tension were simulated, and J was evaluated from the load and load-line displacement.

It was first verified that the resistance is higher in tension than in bending for cracks of the same depth. This result is demonstrated in Figure 3.

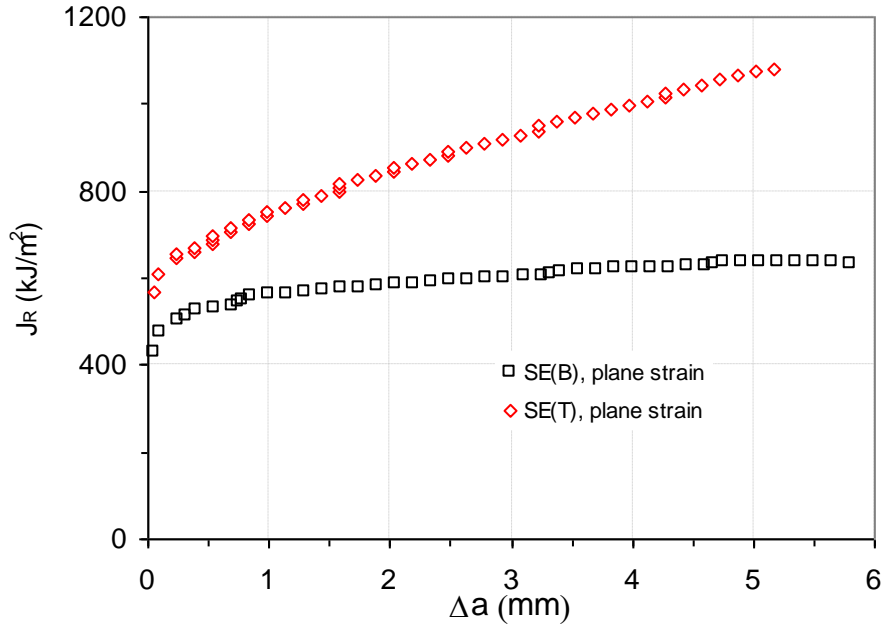


Figure 3. J-resistance curves for 2D SE(B) and SE(T) samples, $a/t=0.5$

Next, the effect of internal pressure on the resistance curve for an internal circumferential flaw ($a/t=0.5$) in a pipe was studied. A power-law stress-strain curve was used with yield strength σ_0 . The effect of a biaxial (hoop) stress σ_b varying from 0 to 90% of σ_0 is shown in Figure 4; parameters of the pipe and flaw were $R_i/t=10$ and $t=40$ mm. Clearly there is negligible influence of biaxial stress on the R curve.

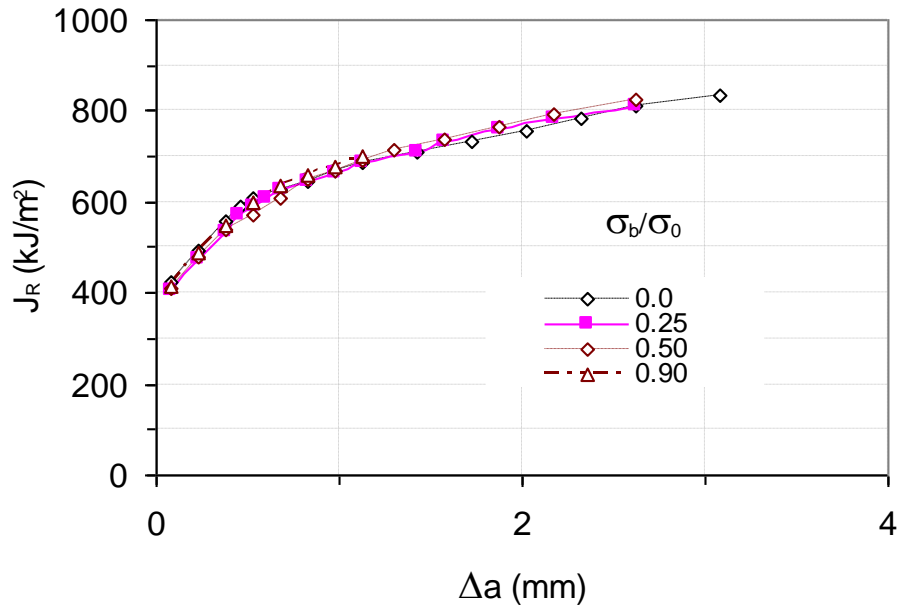


Figure 4. J-resistance curves evaluated for pipe with circumferential crack subjected to axial tension and internal pressure (3D model).

3 FRACTURE TOUGHNESS OF HIGH STRENGTH STEEL PIPE: CONSTRAINT MATCHING [3]

In support of the development of a practical test, FEA was carried out to evaluate the effects of geometry and loading on crack driving force for a flaw in a pipe and for a crack in a single-edge cracked tension (SE(T)) specimen. An important objective was to ensure that the test geometry would reproduce as closely as possible the constraint experienced by a flaw in service. To characterize constraint, among the various parameters that have been proposed, the Q parameter was chosen as the simplest to calculate, easiest to visualize, and the most widely accepted.

Stress fields and constraint parameters of circumferentially-cracked high strength pipe in displacement-controlled tension were compared with those of small-scale specimens loaded in tension and in bending. The crack-tip stress field was found to be of similar form for a circumferential crack in a pipe (Figure 5) and a SE(T) test specimen (Figure 6), while for a SE(B) specimen (Figure 7) there was a significant gradient in the crack-tip stress field. Hence, the fracture toughness could be characterized by only two parameters (e.g. J and Q) for tension-loaded pipe and SE(T) tests, but for SE(B) tests one more parameter was needed to describe the bending term. It was also found that constraint matching was somewhat better for clamped SE(T) specimens than for pin-loaded specimens. Pin-loaded specimens have a larger bending component, which increases constraint. The best constraint matching to circumferential flaws in pipe was found for SE(T) samples with distance between grips of ten times the wall thickness, i.e. $H/W=10$.

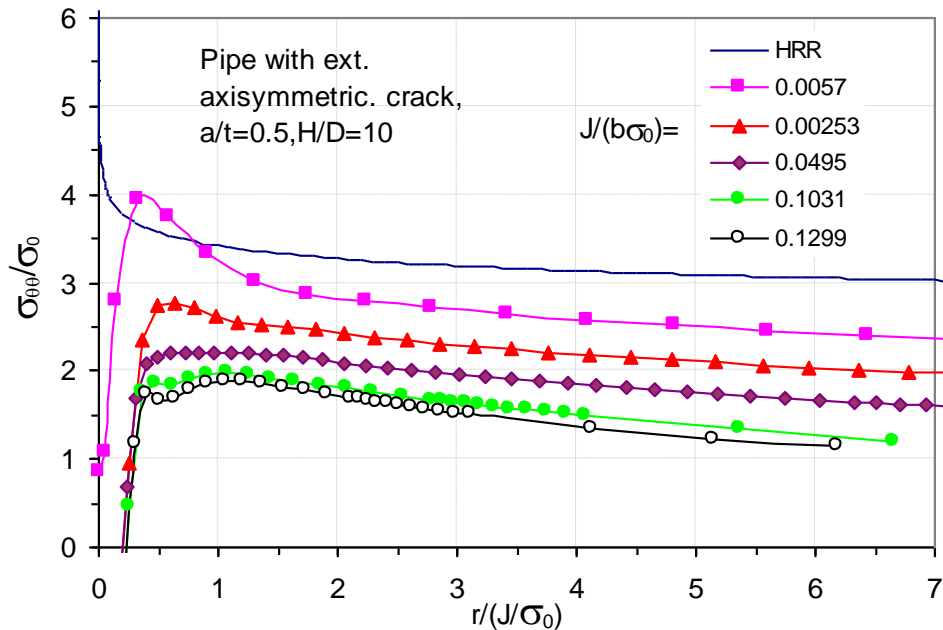


Figure 5. Crack-tip opening stress for an external axisymmetric crack in a pipe (2-D), $a/t=0.5$, $H/D=10$

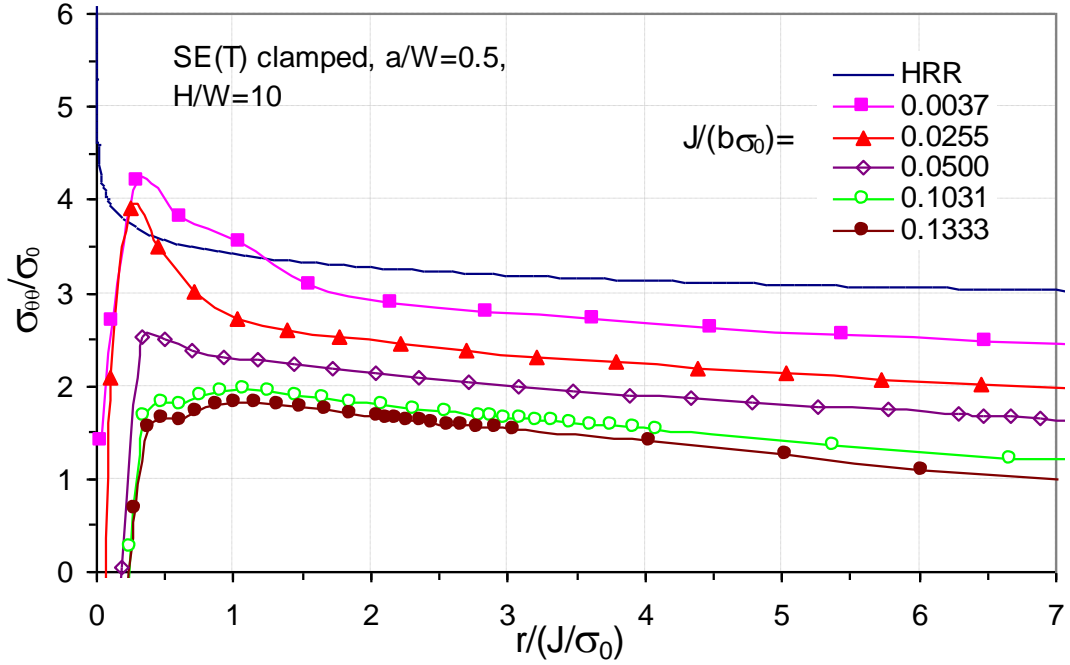


Figure 6. Crack-tip opening stress for SE(T) clamped sample, $a/W=0.5$, $H/D=10$

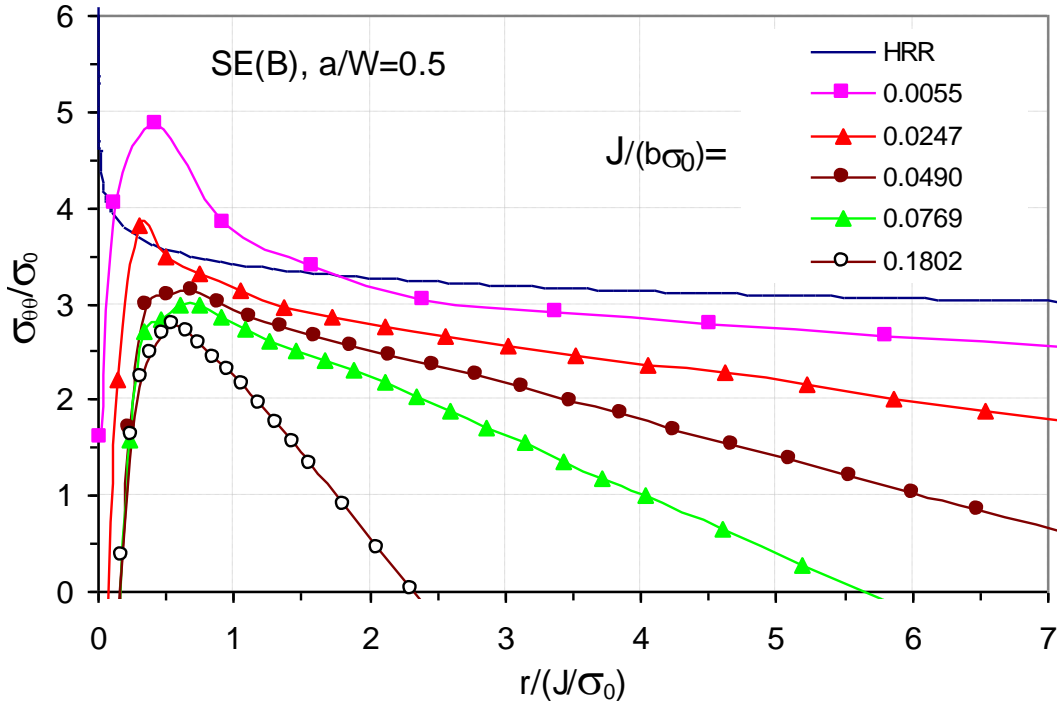


Figure 7. Crack-tip opening stress for SE(B) samples, $a/W=0.5$

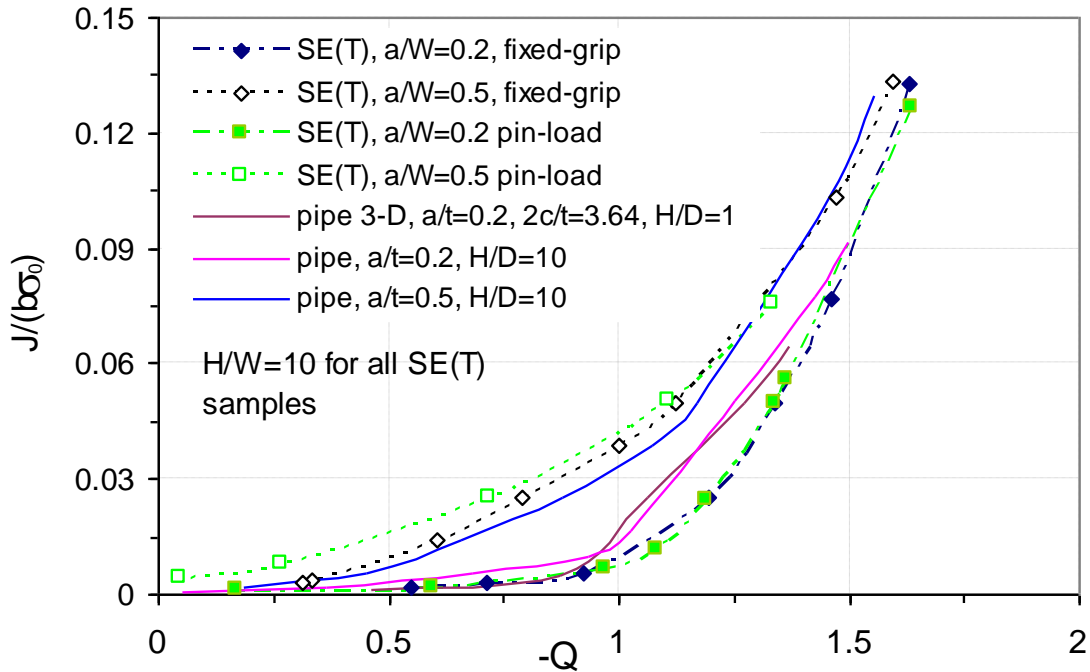


Figure 8. J - Q relations for pipe and SE(T) samples

The gradients of the crack-tip stress field of SE(T) specimens are very close to those of pipes with circumferential flaws. Much steeper gradients exist for SE(B) specimens. For deep cracks, the constraint loss is significantly larger in tension than in bending, at least for moderate J values. The relative crack length of surface flaws in pipe ($2c/t$) was found to have an insignificant effect on constraint for shallow cracks, at least for $2c/t$ greater than about 4.

It was concluded that the constraint in a SE(T) test with ratio of span between load points to width $H/W=10$ provides a reasonable match to that for a circumferential crack in a pipe subjected to tensile loading.

4 CRACK SIZE MEASUREMENT USING UNLOADING COMPLIANCE [4]

Development of a single-specimen SE(T) test requires measurement of crack size during the test. It was decided to use crack-mouth opening displacement (CMOD) elastic unloading compliance for crack size measurement because of the simplicity of this technique and for consistency with ASTM procedures. The assumption is normally made that the unloading compliance depends only on crack size and not on the extent of plastic deformation, so that the unloading compliance of a deformed specimen is the same as the elastic compliance of an undeformed specimen. However, this assumption is not valid for specimens tested in tension because the specimen rotates so that the centre of the remaining ligament moves toward the load line and the unloading compliance is reduced as a result. The deformation of the ligament and specimen rotation is visible in Figure 9. Hence, correction for rotation is required by ASTM E1820 when the unloading compliance technique is used for compact tension (C(T)) specimens, and is also required for SE(T) specimens. A finite element study was undertaken to derive a rotation correction procedure.



Figure 9. SE(T) specimen under load

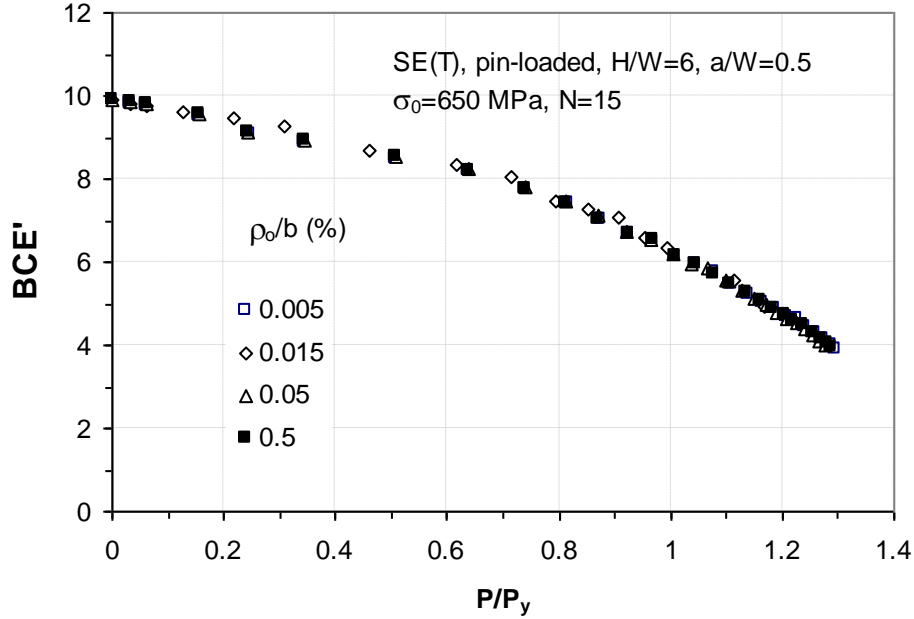


Figure 10. CMOD compliance versus applied load evaluated by FEA

The decrease in compliance with load at a constant crack size is evident from the results shown in Figure 10. At least up to limit load, the compliance change may be approximated by a linear dependence on load. Determination of crack size requires a correction factor for the compliance. It should be noted that, as verified by FEA, compliance rotation correction coefficients for clamped SE(T) specimens are much smaller than those for pin-loaded SE(T) specimens with the same crack size. This is consistent with the prevention of rotation at the ends of clamped specimens.

To obtain the corrected (deformation-free) compliance, FEA calculation showed that for $H/W=10$, where H is the distance between the grips, the measured compliance should be divided by the factor

$$F = 1 - 0.165 \frac{a_0}{W} \left(\frac{P_i}{P_Y} \right)$$

where P_Y is the limit load. Also, to adjust for the presence of side grooves, it was found that an effective thickness B_e should be used where

$$B_e = B - \frac{(B - B_N)^2}{B}$$

Without rotation correction, the compliance is reduced with increasing plasticity at constant crack size which leads to apparent negative crack growth. The effect of applying a rotation correction may be seen by comparing Figure 11 and Figure 12.

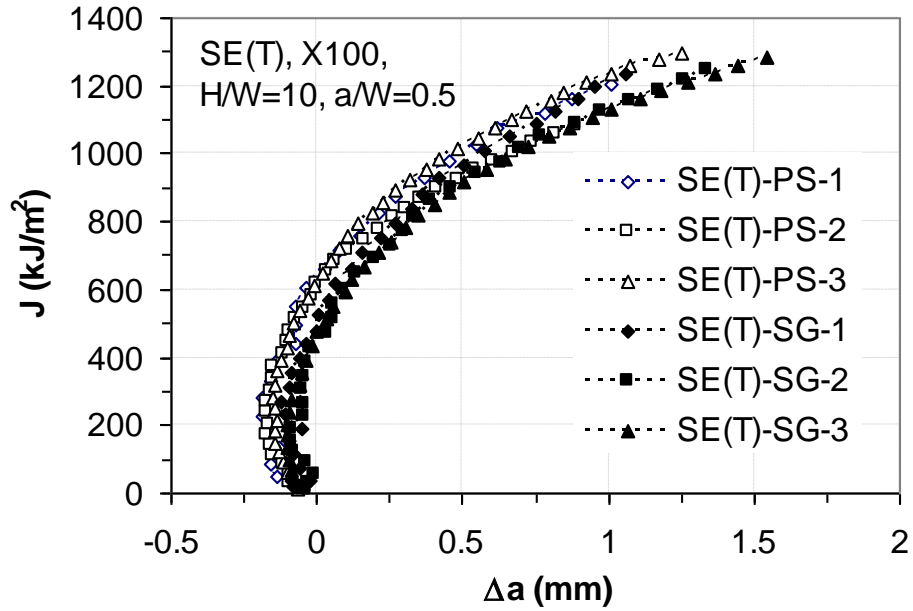


Figure 11. J-R curves for an X-100 pipe steel, no rotation correction, PS: plain-sided; SG: side-grooved

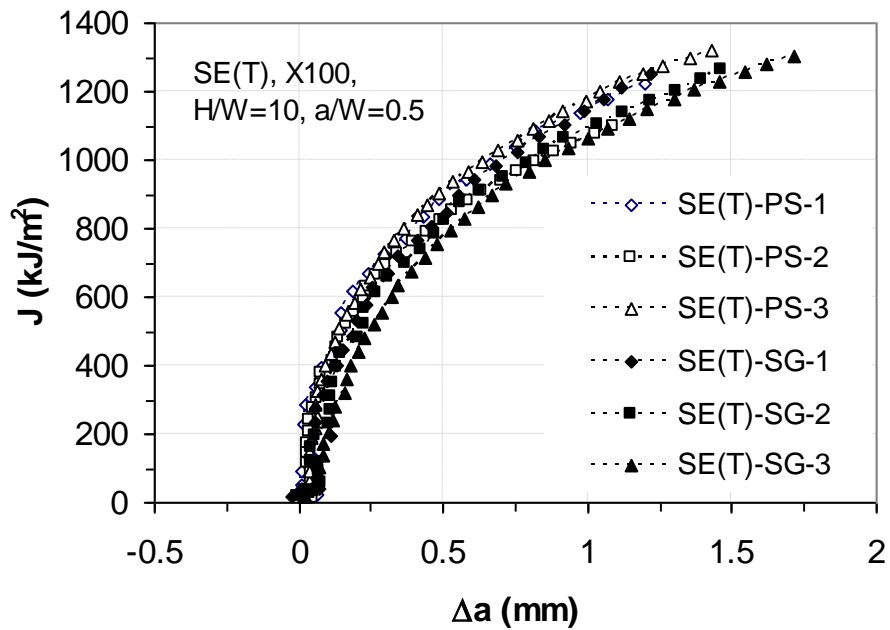


Figure 12. J-R curves for an X-100 pipe steel, with rotation correction and a_{oq} adjustment, PS: plain-sided; SG: side-grooved

5 TRIALS USING SE(T) PROCEDURE [5]

Equations were developed using FEA for evaluation of the J-integral, including correction for crack growth, and incorporated in a test procedure in a format similar to that of ASTM E 1820-06. The evolution of the procedure is reported in a separate publication (MTL 2008-18(TR), “Development of Procedure for Low-constraint Toughness Testing using a Single-Specimen Technique”, Shen, G., J.A. Gianetto and W.R. Tyson, Nov. 2008). The principal equations were reported along with trials of the procedure using specimens of a high-strength pipe steel in a conference publication [5]. SE(T) results were compared with those from conventional SE(B) tests.

As shown in Figure 13, it was verified that the unloading compliance technique gave crack size measurements in very good agreement with nine-point optical measurements on fracture surfaces.

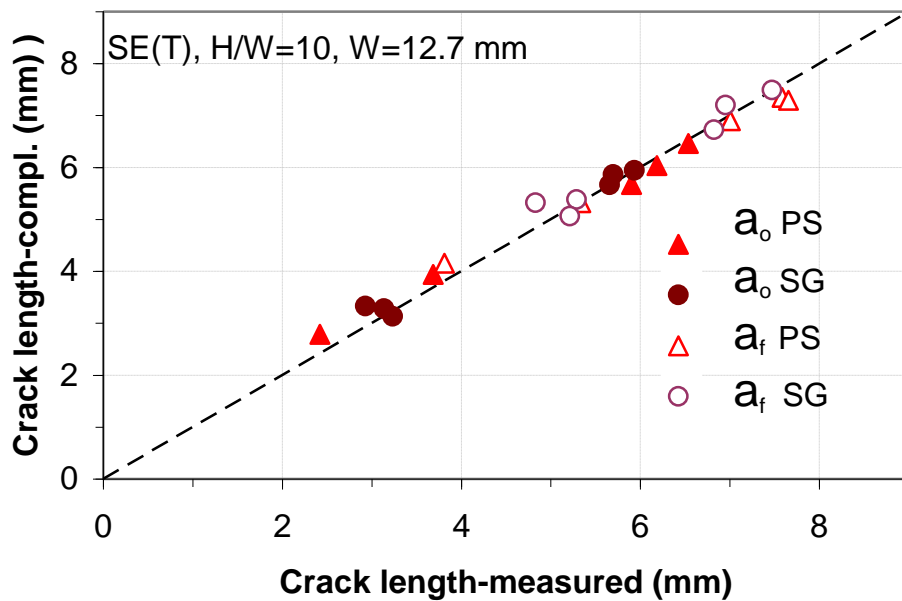


Figure 13. Crack size for clamped SE(T) specimens. a_o , a_f : initial and final crack size (SG: side-grooved, PS: plain-sided)

As shown in Figure 14, crack growth resistance was found to be significantly higher for SE(T) tests (data points) compared with SE(B) tests (solid curves); the presence of side grooves lowered the resistance in both cases, but the difference between tension and bending remained.

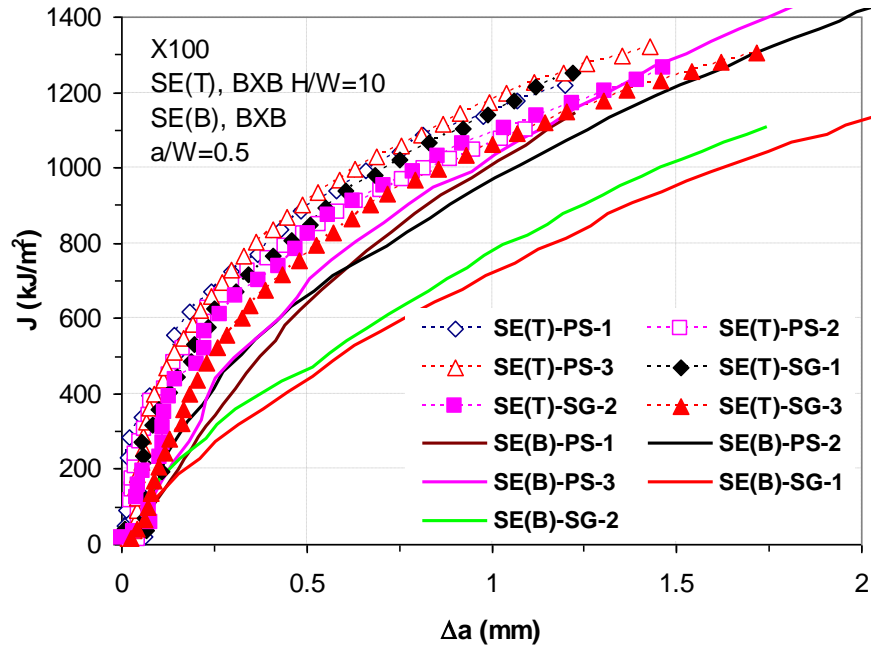


Figure 14. J-R curves measured using SE(T) and SE(B) specimens, $a/W=0.5$

Tests showed that the difference was less pronounced for shallow ($a/W \sim 0.25$) than for deep ($a/W \sim 0.5$) cracks.

Conventional bend tests were also performed for specimens of the same orientation and geometry according to ASTM E1820. Key observations are summarized in Table 1. In particular, note that the toughness for a deep crack in bending is approximately half that for a shallow crack in tension.

Table 1. J values (kJ/m^2) at $\Delta a=0.5$ mm

Specimen type	a/W	PS	SG
SE(B)	0.5	650	450
SE(T)	0.25	1100	900

6 EVALUATION OF CTOD FROM J-INTEGRAL FOR SE(T) SPECIMENS [6]

FEA was used to develop the relationship between J-integral and CTOD for SE(T) specimens, applicable in particular for loads beyond limit load into large-scale yielding which is allowed in strain-based design of pipelines. Note that the largest part of resistance curves for strain-based Engineering Critical Assessment (ECA) is measured at loads above limit load. The equations were developed for homogeneous material. Subsequent work is exploring the applicability of the relations to inhomogeneous material (e.g. welds). J can be measured with considerably less

ambiguity than CTOD, which in the CANMET procedure is obtained experimentally from J and requires a suitable choice of tensile properties; indications are that for mismatch up to ~20 % the equations are acceptable.

There is a one-to-one relationship between J-integral, flow stress (or “effective yield strength”) σ_Y and CTOD δ , commonly expressed for a given material in the form $m=J/(\sigma_Y\delta)$ where m is a parameter dependent primarily on work hardening coefficient and a/W. The value of m was deduced from FEA simulation of SE(T) samples with H/W=10 in clamped loading under small-scale yielding (SSY) and large-scale yielding (LSY) conditions for materials with low to high strain hardening exponents (N=5 to 20), using the 90° intercept definition of δ . Some of the results, for a deep crack, are shown in Figure 15. It was found that, as is evident in Figure 15, that m is independent of load only when the applied load is equal to or less than a reference load $P_Y=B_N(W-a)\sigma_Y$; when $P>P_Y$, the value of m decreases with increasing ligament yield load ratio (P/P_Y). In addition to P/P_Y , it was found that m depends on a/W and work hardening coefficient, N. Equations were derived for evaluation of m for SE(T) specimens with H/W=10 as a function of P/P_Y , N, and a/W from least-squares fits to the FEA data. These equations have been used to obtain δ values from J measured in SE(T) tests.

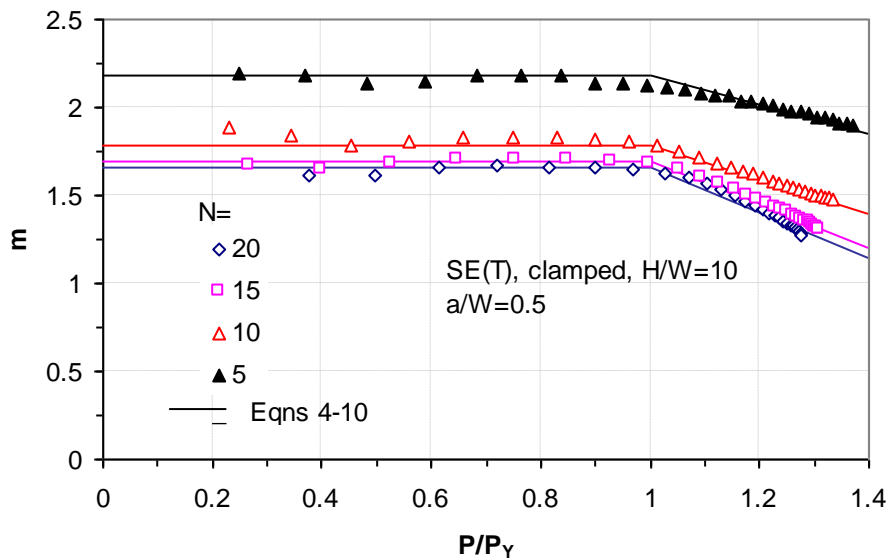


Figure 15. Factor m as function of applied load for a deep crack

Values of m were found also by FEA to relate J to δ for a fully circumferential crack with a/W=0.5 in a pipe. It was found that the m values for the pipe agreed well with those from the equations developed for clamped SE(T) specimens.

The values of m derived in this work were compared with m values for SE(B) specimens in the literature. Results for loads below the reference load are shown in Figure 16, from which it is evident that there is not a great deal of difference in m values at low loads.

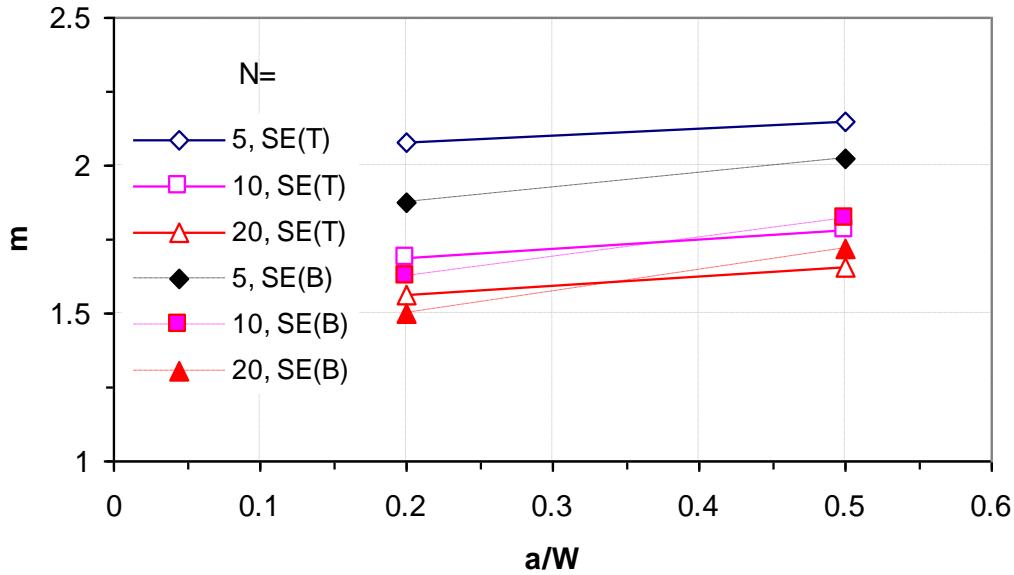


Figure 16. Values of m for SE(T) at load $P \leq P_Y$ and for SE(B) at $\delta_{\max} = a/20$

It should be noted that for most high strength pipe steels, strain-based design requires crack driving force calculation and measurement of resistance to fracture at loads well above P_Y . As a result, the load dependence of m should be taken into account when evaluating CTOD from J . If this is neglected, errors of the order of 25% can be incurred.

7 EFFECT OF SIDE GROOVES [7]

Finite element analysis was conducted to study the effect of side grooves, especially their depth, on CMOD compliance, and distribution of J -integral and crack-tip constraint parameters along the crack front through the thickness of a clamped SE(T) specimen. The study included crack depths of 0.2 and 0.5 W where W is specimen width and side-groove depths of 0, 10% and 20% B where B is specimen thickness, with side-groove root profiles (root radius and angles) within the specifications of ASTM E1820 for SE(B) and compact tension C(T) specimens. 3D results were compared those of plane strain.

Typical results are shown in Figure 17. The J -integral is not constant through the thickness, and the distribution changes with the applied load. The J value (reflecting the crack-tip constraint or stress triaxiality) at low loads is highest near the root of the side grooves for side grooves equal to or greater than 10%, and at the center of the thickness for 0% side-groove depth (plain-sided specimens).

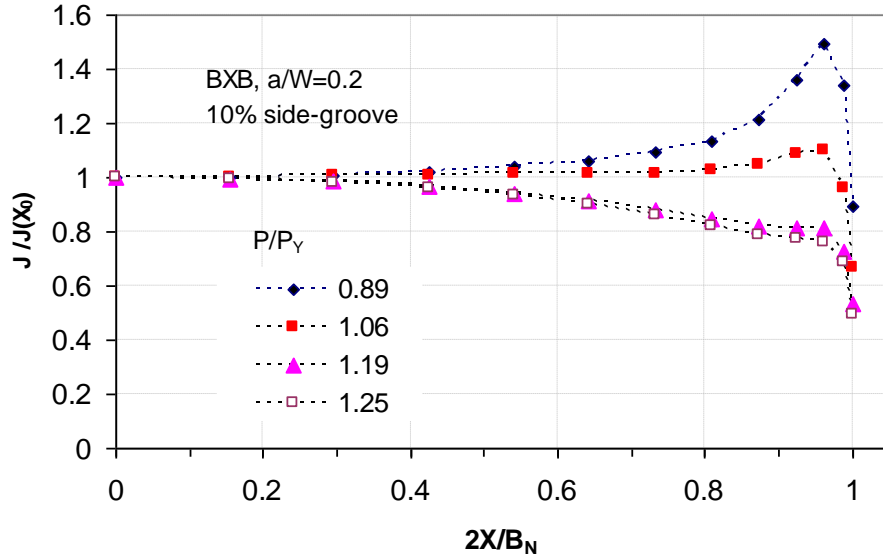


Figure 17. Distribution of J-integral along the crack front , $a/W=0.2$, 10% side grooves

Rather surprisingly, it was also found that the crack-tip constraint with 20% side grooves can be higher than that of a SE(T) specimen with the same crack depth in plane strain. This is doubtless a reflection of the enhanced stress parallel to the crack tip caused by the stress concentration of the side grooves, which has the effect of increasing the stress triaxiality along the crack front. As a result, the J-resistance of a SE(T) specimen with 20% side grooves may be lower than that of the same specimen in plane strain.

Considering both crack-front straightness and constraint matching of side-grooved and plane-strain SE(T) specimens, the optimum side-groove depth was suggested to lie between 10% and 20%.

8 CRACK GROWTH CORRECTION [8]

The recommended practice (MTL 2008-18(TR) includes a correction to the J-integral with a similar basis in theory and similar approximations to the correction used for the SE(B) R curve in ASTM E1820. The approximations are such that closely spaced unloading compliance measurements (i.e. crack size measurements) are required. For comparison with multi-specimen measurements, it was felt desirable to remove this restriction. This can be achieved by modifying the approximations in the derivation of the growth correction. The modifications were reported at ECF18 [6]. Application of the improved procedure is shown in Figure 18 for typical SE(B) test results; the improved procedure is equally applicable to SE(T) results.

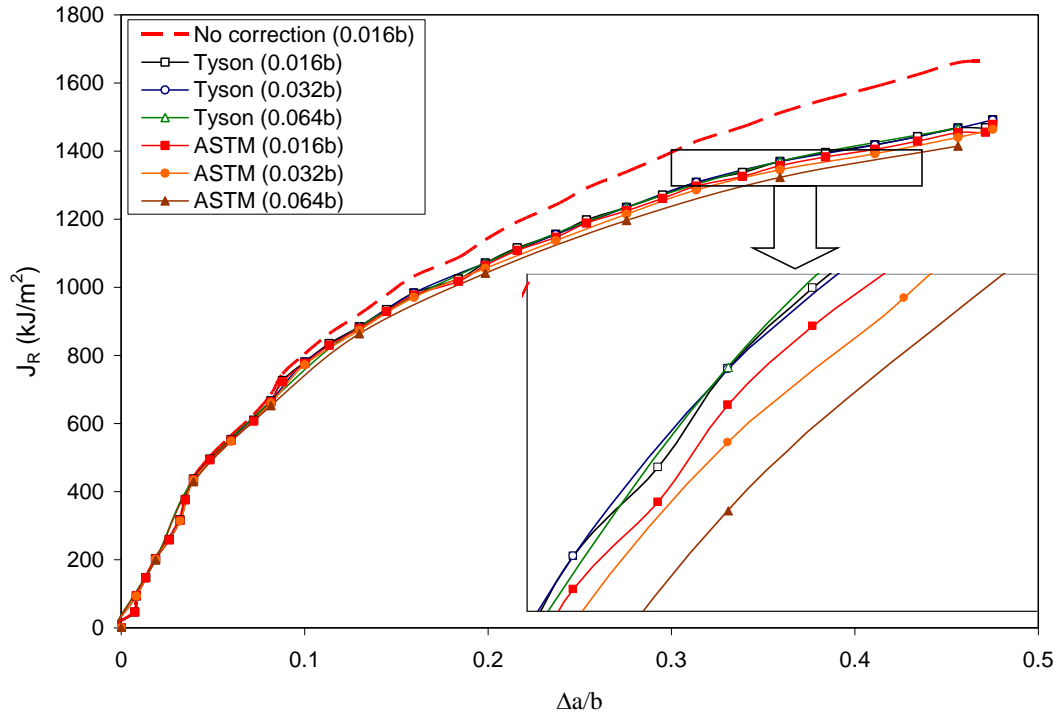


Figure 18. J-resistance curve for X100 pipe steel, with correction for crack growth according to improved procedure (Tyson) and conventional procedure (ASTM) at crack size intervals of 0.016b, 0.032b, and 0.064b

The improved procedure enables crack growth correction of J-resistance curves that retains accuracy even with the use of large intervals between data points (large amount of crack growth between unloadings).

9 FRACTURE TOUGHNESS OF X100 PIPE STEEL: SE(B) AND SE(T) SPECIMENS, ROOM TEMPERATURE AND -20°C [9]

J-resistance testing was performed on SE(T) and SE(B) specimens of X100 pipe steel base material at room temperature and -20°C to further evaluate the SE(T) procedure. The specimens were cracked through-thickness and included two nominal aspect ratios (target $a/W \cong 0.25$ and 0.5). The results showed that shallow-cracked ($a/W \cong 0.25$) bend and tension specimens have higher resistance curves than deeply-cracked ($a/W \cong 0.5$) specimens; ductile propagation was observed at both temperatures. Resistance curves were slightly higher at -20°C than at room temperature for both bending and tension, especially for shallow-cracked specimens. Toughness was significantly lower for specimens with 20% side grooves compared with 10% side grooves and plain-sided specimens.

Crack length predicted from unloading compliance of crack mouth opening displacement for the SE(T) specimens was validated by optical measurement of initial crack length (a_0) and final crack extension ($\Delta a > 1.0$ mm) after heat-tinting, as per ASTM E1820. Predicted crack growths showed acceptable agreement with measured values in all cases. Typical results are shown in Figure 19.

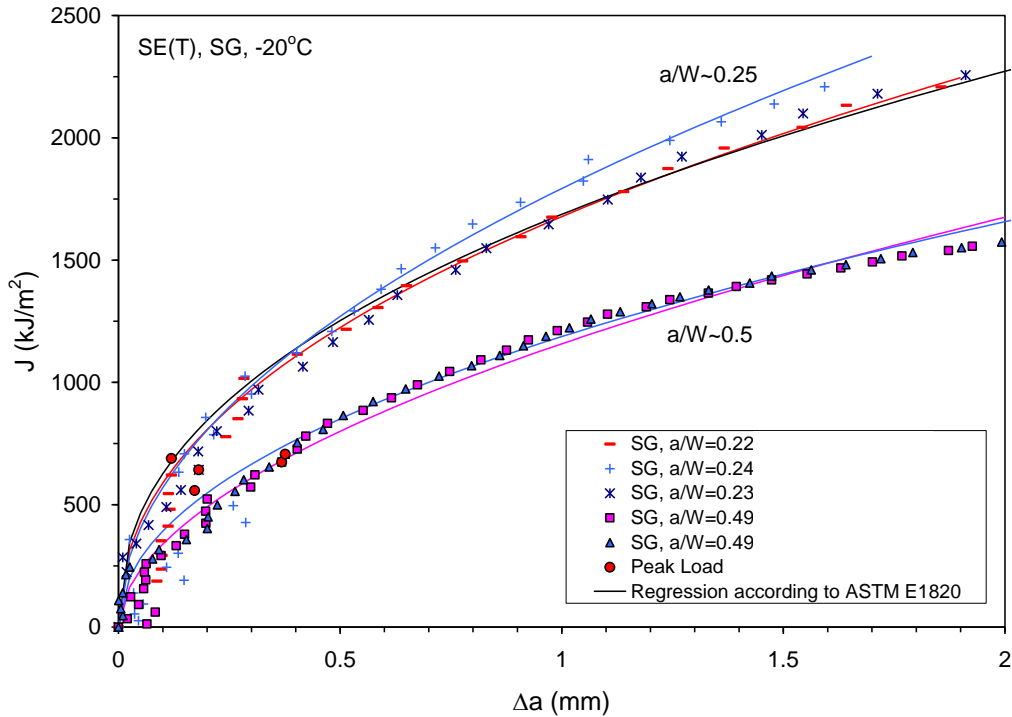


Figure 19. J-resistance curves for SE(T) specimens tested at -20°C, side grooved (SG) 10% (5% on each side)

The effect of side-groove depth on the resistance curve and straightness of the crack front was briefly investigated. For both bending and tension, resistance curves for 10% (total) side-grooved specimens were close to those from plain-sided specimens when other testing conditions, such as pre-crack and testing temperature, were the same. However, 20% (total) side-grooved specimens showed lower toughness. It was occasionally observed that the crack grew faster at the side for 20% side-grooved bend and tension specimens, resulting in crack front concave curvature. For 10% side-grooved specimens a rather straight crack front or slightly faster crack growth in the middle of the specimen (convex curvature) was observed. Some results are shown in Figure 20.

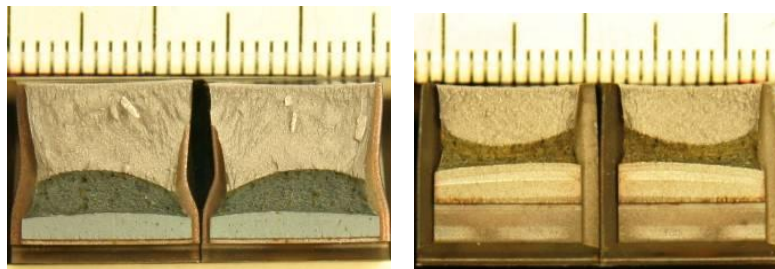


Figure 20. Examples of uneven crack growth in tension specimens: LHS - total 10% side-grooved, shallow-cracked ($a/W \approx 0.25$) specimen and RHS - total 20% side-grooved, deeply-cracked ($a/W \approx 0.5$) specimen. The root radius of side grooves on both specimens is 0.5 mm.

Near initiation, it was found that there was not much difference between toughness in tension and in bending for shallow cracks, as shown in Figure 21. The difference increased with crack depth (Figure 21), in agreement with previous results. The difference in toughness between

tension and bending was little changed with crack growth. Indeed, there is some evidence that the increase in toughness with crack growth is somewhat less in tension than in bending, as evidenced by a somewhat smaller value in tension (~ 0.4) compared with bending (~ 0.5) of the power-law coefficient C_2 in the relation $J = C_1 \Delta a^{C_2}$. However, these conclusions have been somewhat modified as a result of subsequent work reported in final reports 277-T-06 and 277-T-07. The initial analysis for J with SE(B) specimens [9] was performed using load-line displacement (LLD) data. With the recent development of equations using CMOD as was used for SE(T) testing in this project, it became possible to re-analyse the data using CMOD data to generate R curves with the same approach as the SE(T) R curves. When this was done, the difference between tension and bending loading became much more obvious. The conclusion (reported in 277-T-08) was that for the shallow-crack BxB specimens used in this project ($a/W=0.17$ to 0.35) the toughness at 0.5 mm crack growth was higher in tension than in bending.

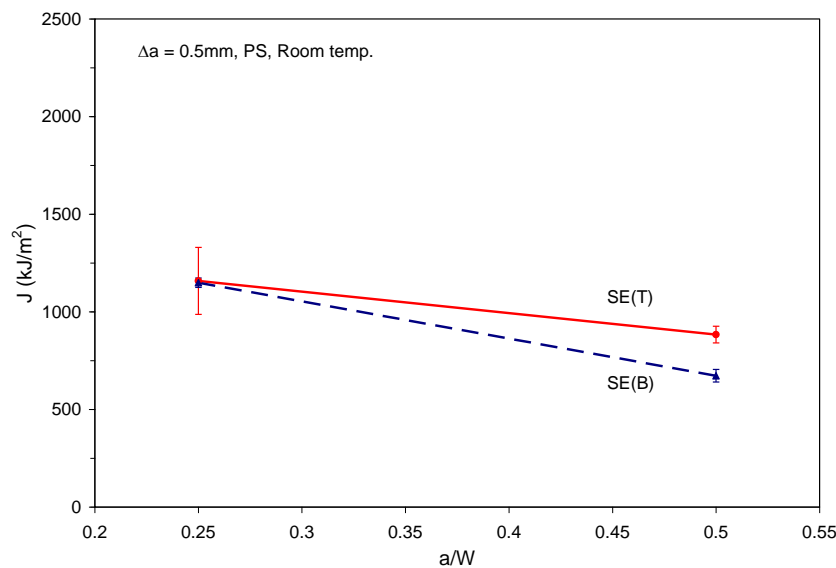


Figure 21. J at $\Delta a=0.5$ mm versus initial crack length ($a/W=0.25$ and 0.5) for plain-sided (PS) tension and bend specimens at room temperature

10 STRETCH ZONE AND BLUNTING LINE [10]

In unpublished work, characteristics of the stretch zone for SE(B) and SE(T) specimens were studied, using laser profilometry and scanning electron microscopy. The measured stretch zone widths (SZWs) of the tension specimens at initiation of tearing were surprisingly found to be much smaller than those of the bend specimens, although the J-integral values at initiation in tension, i.e. at the crack extensions corresponding to the stretch zone widths, are comparable or higher. This was attributed to a dependence of the stretch zone shape on the loading mode.

Finite element simulations showed that the ratio of CTOD to SZW was higher for SE(T) specimens than for SE(B) specimens. The crack tip was found to blunt to a nearly semi-circular shape for SE(B) specimens, but that blunting was more acute (less crack advance for a given CTOD) for SE(T) specimens. This has significant implications for the blunting line. The blunting line may be written as $J=(k m \sigma_Y) \Delta a$ where $k=2 \tan \theta$ is a geometric parameter relating the CTOD δ to the crack advance Δa : $\tan \theta=(\delta / 2) / \Delta a$ (θ is the tilt angle of the stretch zone). Values of $2 \tan \theta$

measured in this study and reported in the literature are given in Table 2. From the present work, $k \approx 1.8$ for SE(B) and ≈ 2.4 for SE(T). Values of m are more sensitive to work hardening coefficient N than to a/W ; for $N \sim 20$, typical of high-strength steels, m ranges from 1.5 to 1.6 for both SE(T) and SE(B) specimens. Taking $m \sim 1.6$, the slope of the blunting line $J/\Delta a = km\sigma_Y$ for SE(B) is $\sim 2.9\sigma_Y$ and for SE(T) is $\sim 3.8\sigma_Y$. This indicates that the blunting line should be somewhat steeper for both SE(B) and SE(T) specimens than the value of $2\sigma_Y$ assumed in ASTM E1820.

Table 2. Values of $2\tan\theta$ ($=k$)

Test type	Specimen condition*	$k = 2\tan\theta$				
		Measurements in this study	ASTM	JSME	BS 7448	ESIS
SE(B)	SG, SC	2.01	2	1.4-2	2.31**	2.5
	PS, SC	2.05				
	SG, DC	1.77				
	PS, DC	1.74				
SE(T)	SG, SC	2.24	n/a	n/a	n/a	n/a
	PS, SC	2.57				
	SG, DC	2.42				
	PS, DC	2.39				
C(T)	n/a	n/a	2	1.4-2	2.31**	2.5

* PS: plain-sided, SG: side-grooved, SC: shallow-cracked, DC: deep-cracked, n/a: not applicable

** For steel in this study

11 SUMMARY

The ten papers outlined in this report have described the development and application of a single-specimen single-edge tension SE(T) test. This work has led to a Recommended Practice, which is currently (2011) being evaluated in a multi-laboratory international round robin.

The Recommended Practice refers only to homogeneous material, but the method has been applied to characterization of welds. The complications introduced in testing the inhomogeneous welds include: notch placement; definition of tensile properties, especially in conversion from J to CTOD; residual stress, which affects fatigue crack straightness as well as crack growth; and crack growth path, which for the HAZ is unlikely to be in the same plane as the pre-crack. Experience with these issues will be reported separately.

12 REFERENCES

1. Shen, G., and W.R. Tyson, "Effect of biaxial stress on crack driving force", Proc. ASME Pressure Vessels and Piping Conference, paper PVP2006-ICPVT-11-93849, Vancouver, July 23-27, 2006.
2. Tyson, W.R., G. Shen and G. Roy, "Effect of biaxial stress on ECA of pipelines under strain-based design", Proc. International Society of Offshore and Polar Engineers (ISOPE 2007), Lisbon, July 2-6, 2007.
3. Shen, G., R. Bouchard, J.A. Gianetto and W.R. Tyson, "Fracture toughness evaluation of high-strength steel pipe", PVP2008-61100, Proc. ASME PVP 2008 Conf., Chicago, July 2008.
4. Shen, G. and W.R. Tyson, "Crack size evaluation using unloading compliance in single-specimen single-edge-notched tension fracture toughness testing", Jour. of Testing and Evaluation Vol. 37 (4), paper ID JTE102368, ASTM, 2009
5. Shen, G., J.A. Gianetto and W.R. Tyson, "Measurement of J-R curves using single-specimen technique on clamped SE(T) specimens", Proc. 18th Int. Offshore and Polar Engineering Conf., Osaka, Japan, 21-26 June 2009.
6. Shen, G. and W.R. Tyson, "Evaluation of CTOD from J-integral for SE(T) Specimens", Pipeline Technology Conference, Ostend, Belgium, 12-14 October 2009.
7. Shen, G., W.R. Tyson, J.A. Gianetto and D.-Y. Park, "Effect of side grooves on compliance, J-integral and constraint of a clamped SE(T) specimen", PVP2010-25164, ASME Pressure Vessel and Piping Division Conference PVP2010, Seattle, Washington, USA, July 18-22, 2010.
8. Tyson, W.R., D.-Y. Park and G. Shen, "Improved crack growth correction for resistance curve determination", Fracture of Materials and Structures from Micro to Macro Scale, ECF18, Dresden, Germany, August 30 to September 3, 2010.
9. Park, D.-Y., W.R. Tyson, J.A. Gianetto, G. Shen and R.S. Eagleson, "Evaluation of fracture toughness of X100 pipe steel using SE(B) and clamped SE(T) single specimens", IPC2010-31282, 8th International Pipeline Conference IPC2010, September 27 – October 1, 2010, Calgary, Alberta, Canada
10. Park, D.-Y., G. Shen, W.R. Tyson, J.A. Gianetto and R.S. Eagleson, "Effect of loading mode on the stretch zone shape for SE(B) and SE(T) specimens", unpublished work, CANMET Materials Technology Laboratory, 2010.